Available online at www.sciencedirect.com
SCIENCE DIRECT®
Journal of Solid State Chemistry 177 (2004) 1829–1837
JOURNAL OF SOLID STATE CHEMISTRY
http://elsevier.com/locate/jssc

A comparative study of the Aurivillius phase ferroelectrics $CaBi_4Ti_4O_{15}$ and $BaBi_4Ti_4O_{15}$

J. Tellier, Ph. Boullay,* M. Manier, and D. Mercurio

Laboratoire de Sciences des Procédés Céramiques et Traitements de Surface, Faculte des Sciences et Techniques, SPCTS-CNRS UMR6638, 123 Av. Albert Thomas, Université de Limoges, F-87060 Limoges Cedex, France

Received 13 November 2003; received in revised form 18 December 2003; accepted 7 January 2004

Abstract

The room temperature structures of the four-layer Aurivillius phase ferroelectrics $CaBi_4Ti_4O_{15}$ and $BaBi_4Ti_4O_{15}$ are determined by means of single crystal X-ray diffraction. Regarding the $CaBi_4Ti_4O_{15}$ phase, in agreement with the tolerance factor, a significant deformation of the perovskite blocks is observed. The rotation system of the octahedra is typical from even layer Aurivillius phases and leads to the use of the space group $A2_1am$. For the $BaBi_4Ti_4O_{15}$ phase, only a weak variation with respect to the $F2mm$ space group can be suggested from single crystal X-ray diffraction. A significant presence of Ba atoms in the $[M_2O_2]$ slabs is confirmed in agreement with the previous works but specific Ba^{2+} and Bi^{3+} sites have to be considered due to the large difference in bounding requirement of these cations. Possible origins for the ferroelectric relaxor behavior of the Ba-based compound are discussed in view of the presented structural analyses.

1. Introduction

The ferroelectric properties of the Aurivillius type compounds currently arouse a keen interest because of their potential application in the realization of ferroelectric nonvolatile memories (Fe-RAM). This family of bismuth oxides, discovered more than 50 years ago by Aurivillius [1], can be described as resulting from the regular stacking of $[M_2O_2]^{2+}$ slabs and $[A_{n-1}B_nO_{3n+1}]^{2-}$ perovskite blocks. While the perovskite blocks offer large possibilities in terms of compositional flexibility, the cation sites in the interleaved $[M_2O_2]$ slabs are almost exclusively occupied by Bi^{3+} cations forming $[Bi_2O_2]^{2+}$ slabs. Crystallographic studies have demonstrated the key role of the A-site cation in the ferroelectric behavior of these materials [2] and, at first approximation, a direct relation between the average ionic radii of the A-site cation and the temperature of the ferroelectric–paraelectric transition (T_c) can be established [3]. Apart from the polar displacements, the ferroelectric phases are also characterized by cooperative tiltings of the BO_6 octahedra. In a recent paper, we have shown that actually these structural features are common to all Aurivillius ferroelectric phases and can be described in a unified approach using the $(3+1)D$ superspace group formalism for members $n = 2-\infty$ [4].

One interesting feature of the Aurivillius phases resides in the compositional flexibility of the perovskite blocks which allows to incorporate various cations such as Na^+, K^+, Ca^{2+}, Sr^{2+}, Ba^{2+}, Pb^{2+}, Bi^{3+} or Ln^{3+} for the A-site and Fe^{3+}, Cr^{3+}, Ti^{4+}, Nb^{5+} or W^{6+} for the B-site. It is thus possible to modify the ferroelectric properties according to the chemical composition. As an illustration, the majority of the Aurivillius oxides where A = Ba have a relaxor type ferroelectric behavior to the difference of their analogues where A = Sr, Ca and Pb. Although this phenomenon was observed since many years, its structural origin is not yet clearly elucidated. In the present paper we present the comparative single crystal X-ray diffraction structural study of both $CaBi_4Ti_4O_{15}$ and $BaBi_4Ti_4O_{15}$ (members $n = 4$). These two compounds are interesting in the sense they represent two limit cases considering the average ionic radii of the A-site cation as it will be discussed further on. To our knowledge no recent structural determination has been published for $CaBi_4Ti_4O_{15}$. For $BaBi_4Ti_4O_{15}$, in the last 2 years, not less than four articles have reported its crystal structure determination

*Corresponding author. Fax: +33-5-55-45-72-70.
E-mail address: philippe.boullay@unilim.fr (P. Boullay).

0022-4596/$ - see front matter © 2004 Elsevier Inc. All rights reserved.
doi:10.1016/j.jssc.2004.01.008

based on powder diffraction data obtained from various sources: laboratory X-ray [5], synchrotron X-ray [6–7] and Neutron experiments [7–8]. Nonetheless all these studies disagree and we believe that the structural determination of these compounds needs further investigations.

2. Experimental

Samples were prepared by solid-state reaction in a molten salt. Stoichiometric quantities of $CaCO_3$, $BaCO_3$, Bi_2O_3 and TiO_2 were intimately mixed in the 1:1 molar proportion with eutectic compound NaCl + KCl and then sintered in air at 800°C for 1 h. After an aqueous washing, the formation of the phase and the quality of the powder (monophasic sample) was confirmed using a Guinier camera. Single crystals were grown using a flux method in an excess of Bi_2O_3. The obtained powders and Bi_2O_3 were mixed in the 1:4 molar proportion and placed in a platinum crucible for the following thermal treatment: heating up to 1150°C at 300°C per hour, dwelling at 1150°C for 5 h, cooling down to 500°C at 3°C per hour and finally cooling to room temperature.

Transparent crystals in the form of thin platelets were extracted from solidified materials using hydrochloric acid and then washed in hot water. They have been observed by optical microscopy under polarized light in order to pre-select those which presented only one ferroelastic domain.

Chosen crystals were studied using a Siemens–Bruker KAPPA-CCD four circle diffractometer equipped with a CCD detector and using the graphite-monochromatized Mo$K\alpha$ wavelength. Intensities were extracted from the recorded images using the "Ewald CCD" software suite. The examination of the reciprocal space by means of reconstructions of precession photographs was used to choose the two crystals retained for this study. Further details about the data collection are given in Table 1.

The intensities were corrected for Lorentz-polarization effects and absorption corrections were applied using the Gaussian method. The shape of the crystal was obtained using a CCD camera mounted on the KAPPA-CCD diffractometer. These corrections and the crystal structure analysis were performed using the JANA2000 software [9].

Table 1
Crystal data for $CaBi_4Ti_4O_{15}$ and $BaBi_4Ti_4O_{15}$ measured using a Siemens–Bruker Kappa-CCD four circle diffractometer

Formula	$CaBi_4Ti_4O_{15}$	$BaBi_4Ti_4O_{15}$
Space group	$A2_1am$ (No. 36-cba)	$F2mm$ (No. 42-cab)
Cell parameters (Å)[a]		
	$a = 5.4234(2)$	$a = 5.4433(4)$
	$b = 5.4021(5)$	$b = 5.4319(6)$
	$c = 40.5935(3)$	$c = 41.6941(6)$
Z, density (g/cm^3)	4, 7.309	4, 7.569
Crystal size (μm^3)	$98 \times 147 \times 5$	$59 \times 93 \times 4$
Wavelength (Å)	0.71073 (Mo$K\alpha$)	
Monochromator	Graphite	
θ range (°)	1–32.5	1–26.2
F (0 0 0)	2240	2384
Reflections measured	5711	4252
Reflections unique	2996	691
Rint [$I > 3\sigma(I)$]/[all]	3.53%/3.63%	3.57%/3.71%

[a] Refined against the whole of the collected data.

3. Results

3.1. Crystal structure of $CaBi_4Ti_4O_{15}$

The whole of the collected data were analyzed firstly visually using the reconstruction of precession photographs (see the $(0kl)^*$ plane as a representative illustration in Fig. 1a) and secondly by a systematic check on all measured intensities using Maxus which is a part of the "Ewald CCD" software suite. Both approaches lead unambiguously to the use of the space group $A2_1am$ (SG No. 36-setting cba) in agreement with the possibilities predicted by the general model developed in [4] and with the space group of the related compound $SrBi_4Ti_4O_{15}$ [10]. Regarding the Sr/Bi repartition, this study has shown that no significant occupancy of the $[M_2O_2]$ slabs by Sr is observed and that the two A-sites of the perovskite blocks are randomly occupied by Sr (fixed to 0.67Bi/0.33Sr).

Considering the large difference in the scattering factors for Ca^{2+} and Bi^{3+} cations, the Ca/Bi occupancy of the two A-sites was determined from experimental data with a good confidence on the results. Attempts to incorporate Ca inside the $[M_2O_2]$ slabs give no significant evidence (percentage of Ca atoms eventually present are beyond the refinement uncertainties). The possibility to separate Ca and Bi atomic positions for the mixed occupied sites—Bi/Ca(2) and Bi/Ca(3)—was also tested and again no evidence of such a tendency is observed as confirmed by the low thermal displacement parameters obtained for these two sites. The results obtained at the final stage of the single crystal X-ray refinement are summarized in Table 2. The main interatomic distances in the coordination sphere of the cationic sites are given in Table 3. A representation of the crystal structure projected onto the $(y0z)$ and $(x0y)$ planes are presented, respectively, in Figs. 2 and 3.

3.2. Crystal structure of $BaBi_4Ti_4O_{15}$

The recent works [5–8] propose a scattered view of the crystal structure of this compound. One of this work [5] indicates a $I4/mmm$ space group while the others [6–8]

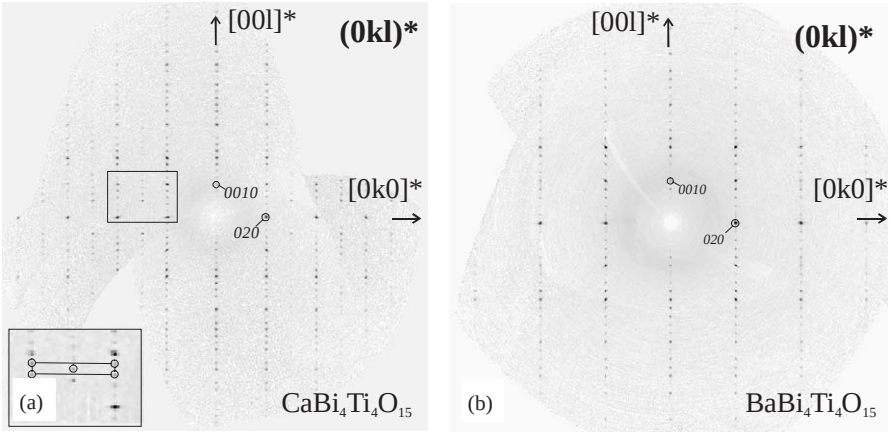

Fig. 1. Reconstruction of the $0\,k\,l$ precession photographs based on the single crystal X-ray data collection obtained for (a) $CaBi_4Ti_4O_{15}$ and (b) $BaBi_4Ti_4O_{15}$. In (a), reflections obeying to the condition $0\,k\,l: k+l=2n$, and compatible with a A lattice centering, are visible for $CaBi_4Ti_4O_{15}$. As illustrated in (b) such reflections are not observed for $BaBi_4Ti_4O_{15}$ as expected for an F lattice centering.

Table 2
Refined structural parameters for $CaBi_4Ti_4O_{15}$ at 25°C $A2_1am$ (No. 36) with $a = 5.4234(2)$ Å, $b = 5.4021(5)$ Å, $c = 40.5935(3)$ Å. R indices [$I > 3\sigma(I)$/all data]: $R = 4.03\%/4.94\%$ and w$R = 4.59\%/4.63\%$

	Wickoff	x	y	z	U_{iso}/U_{eq}	Occupancy
Bi(1)	8*b*	0.25[a]	0.2698(1)	0.21897(1)	0.01242(9)	1
Bi/Ca(2)	4*a*	0.2464(4)	0.2520(1)	0	0.01130(19)	0.60(1)/0.40(1)
Bi/Ca(3)	8*b*	0.2452(3)	0.2438(1)	0.89559(1)	0.01175(13)	0.70(1)/0.30(1)
Ti(1)	8*b*	0.2148(5)	0.2478(2)	0.54921(4)	0.0058(3)	1
Ti(2)	8*b*	0.2155(4)	0.2475(2)	0.34815(4)	0.0053(3)	1
O(1)	4*a*	0.679(2)	0.3250(10)	0	0.0087(17)	1
O(2*a*)	8*b*	0.4735(10)	0.4678(10)	0.5402(2)	0.0112(14)	1
O(2*b*)	8*b*	0.4014(10)	−0.0470(10)	0.5523(2)	0.0093(13)	1
O(3)	8*b*	0.986(2)	0.496(2)	0.25022(10)	0.0084(11)	1
O(4)	8*b*	0.1915(10)	0.3106(10)	0.4048(2)	0.0118(13)	1
O(5*a*)	8*b*	0.4304(10)	0.5282(10)	0.3528(2)	0.0106(14)	1
O(5*b*)	8*b*	0.4683(10)	0.0142(10)	0.36119(10)	0.0075(13)	1
O(6)	8*b*	0.215(2)	0.1976(10)	0.6951(2)	0.0183(15)	1

Anisotropic thermal displacement parameters

	U_{11}	U_{22}	U_{33}	U_{12}	U_{13}	U_{23}
Bi(1)	0.01505(19)	0.00893(13)	0.01330(15)	0.0003(5)	−0.0011(3)	−0.00251(11)
Bi/Ca(2)	0.0082(4)	0.0099(3)	0.0158(3)	−0.0001(7)	0	0
Bi/Ca(3)	0.0135(3)	0.00754(18)	0.0142(2)	0.0007(5)	0.0046(4)	0.00084(13)

Fractional coordinates and thermal parameters (Å^2).
[a] Fixed coordinate (polar space group).

indicate a $F2mm$ space group, based both on synchrotron powder X-ray diffraction [6–7] and on neutron powder diffraction (NPD) data [8]. In [7], a supplementary NPD experiment indicates the space group $A2_1am$ as the correct one. Most of these studies (except [8]) agree with the necessity to incorporate Ba inside the $[M_2O_2]$ slabs but the ratios given for the mixed Ba/Bi sites are different.

The analysis of the data obtained from the $BaBi_4Ti_4O_{15}$ single crystal was carried out in a way similar to that of $CaBi_4Ti_4O_{15}$. The reconstruction of sections of the reciprocal space (see the $(0kl)^*$ plane in Fig. 1b) and the systematic analysis of the collected intensities indicates both that this compound crystallizes in the space group $F2mm$ (SG No. 42-setting cab) with $a > b$. This answers to the ambiguity raised in [8] about the direction of the polar axis. It should be noted that several crystals were tested to check this result and that some presented few very diffuse nodes localized on positions compatible with the space group $A2_1am$. In order to obtain complementary informations, Selected Area Electron Diffraction (SAED) experiments were performed on a powder sample using a JEOL 2010 electron microscope. The SAED reveals a certain

inhomogeneity of the sample with patterns exhibiting either extra spots and/or diffuse streaks (Fig. 4). These extra spots are compatible with the $A2_1am$ space group and the diffuse scattering, when present, is always associated to reciprocal rows specific to this space group. The fact that one of the NPD studies [7] also indicates a space group $A2_1am$ let us suppose that only the oxygen atoms deviate slightly from the $F2mm$ symmetry. Thus, at first, we chose to refine the X-ray diffraction data considering the $F2mm$ space group.

At a first stage of the refinement only the A-sites of the perovskite blocks were considered to have a mixed occupancy. Attempts to incorporate Ba inside the $[M_2O_2]$ slabs (refined value close to 10%) actually lead to a significant reduction of the reliabilities factors (R_{obs} drops from 5.28% to 4.84%) in agreement with the above mentioned works [5–7]. Contrary to the refinement proposed in [6], titanium and oxygen thermal coefficients show stability and were refined independently. Regarding the atomic positions, the crystal structure is close to the one obtained in [6] but high thermal displacement parameters are obtained for some oxygen positions and all the A-sites (anisotropic displacements). When one assumes a mixed Ba/Bi occupancy for all A-sites, it is quite difficult to admit that these two cations have the same environment. Notably, the atomic position associated to the $[M_2O_2]$ slabs shows characteristics undoubtedly related to Bi^{3+}

Table 3
Main interatomic distances in the coordination sphere (<3 Å) of Bi, Bi/Ca and Ti atomic positions obtained from the $CaBi_4Ti_4O_{15}$ structure refinement

Ti(1)–O(1)	2.045(2) Å × 1	Ti(2)–O(4)	2.329(8) Å × 1
Ti(1)–O(2*a*)	2.049(6) Å × 1	Ti(2)–O(5a)	1.920(6) Å × 1
Ti(1)–O(2*a*)	1.878(6) Å × 1	Ti(2)–O(5a)	1.976(6) Å × 1
Ti(1)–O(2*b*)	2.022(6) Å × 1	Ti(2)–O(5b)	1.936(6) Å × 1
Ti(1)–O(2*b*)	1.890(6) Å × 1	Ti(2)–O(5b)	2.019(6) Å × 1
Ti(1)–O(4)	1.902(8) Å × 1	Ti(2)–O(6)	1.776(8) Å × 1
Bi(1)–O(3)	2.270(9) Å × 1	Bi/Ca(3)–O(4)	2.386(6) Å × 1
Bi(1)–O(3)	2.295(9) Å × 1	Bi/Ca(3)–O(4)	2.464(6) Å × 1
Bi(1)–O(3)	2.409(10) Å × 1	Bi/Ca(3)–O(2b)	2.543(7) Å × 1
Bi(1)–O(3)	2.201(9) Å × 1	Bi/Ca(3)–O(5a)	2.320(7) Å × 1
Bi(1)–O(6)	2.515(6) Å × 1	Bi/Ca(3)–O(5a)	2.845(7) Å × 1
Bi(1)–O(6)	2.707(11) Å × 1	Bi/Ca(3)–O(5b)	2.354(5) Å × 1
		Bi/Ca(3)–O(5b)	2.433(5) Å × 1
Bi/Ca(2)–O(2*b*)	2.528(8) Å × 2		
Bi/Ca(2)–O(2*a*)	2.557(7) Å × 2		
Bi/Ca(2)–O(2*a*)	2.501(7) Å × 2		
Bi/Ca(2)–O(1)	2.379(11) Å × 1		
Bi/Ca(2)–O(1)	2.314(6) Å × 1		

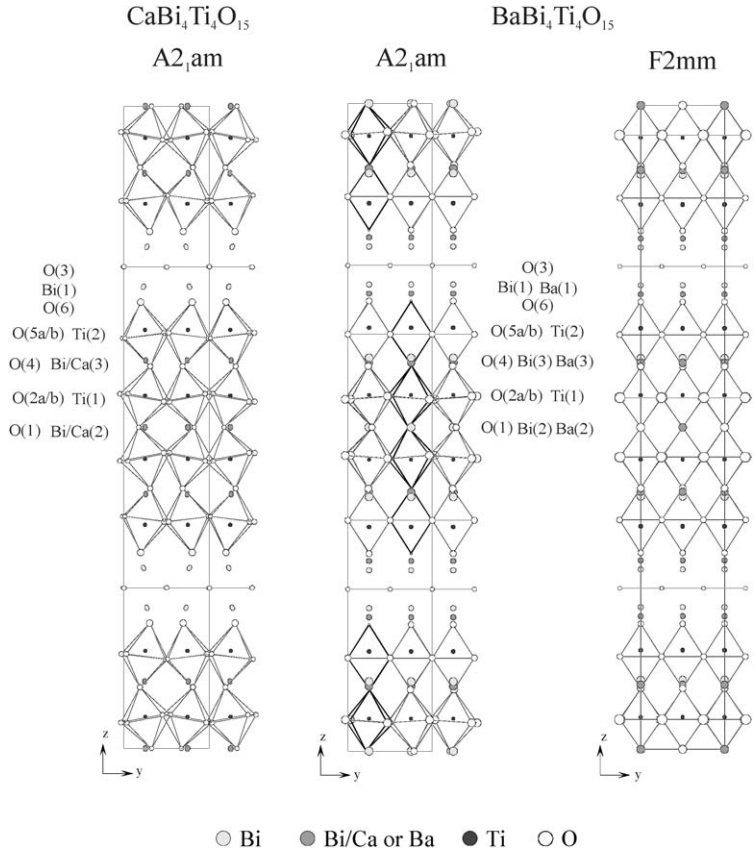

Fig. 2. Crystal structures of $CaBi_4Ti_4O_{15}$ and $BaBi_4Ti_4O_{15}$ projected onto the ($y0z$) plane. The size of the spheres or ellipsoids used to represent the atomic positions correspond, respectively, to the isotropic or anisotropic thermal displacement parameters.

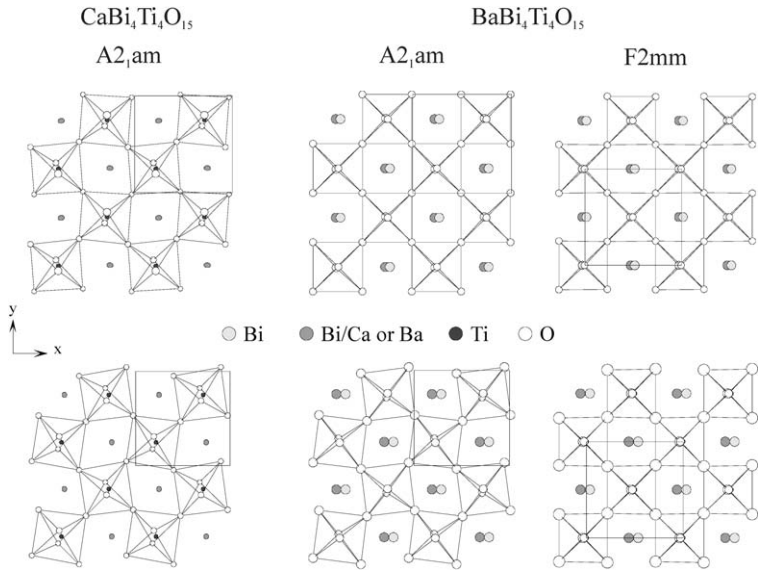

Fig. 3. Comparison of the distortion of the perovskite blocks in $CaBi_4Ti_4O_{15}$ and $BaBi_4Ti_4O_{15}$ projected onto the ($x0y$) plane. In the upper and lower parts are represented, respectively, the external and internal part of the $n = 4$ perovskite blocks. The size of the spheres or ellipsoids used to represent the atomic positions correspond, respectively, to the isotropic or anisotropic thermal displacement parameters.

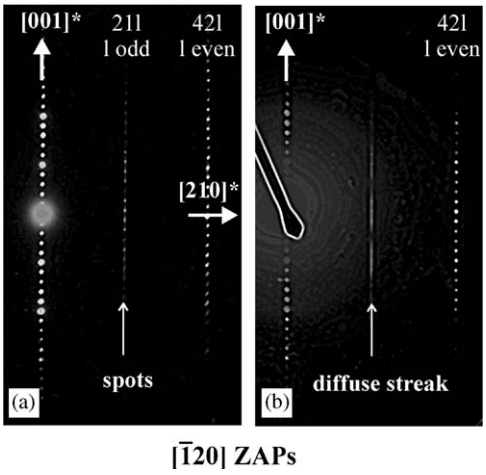

Fig. 4. Part of [−120] Zone Axis Patterns obtained for $BaBi_4Ti_4O_{15}$ in (a) spots compatible with A lattice centering are clearly visible while in (b) only a diffuse streak is observed.

environment (four short Bi–O distances) which are incompatible with Ba–O distances. Thus the possibility to separate Ba and Bi atomic positions for all the three mixed occupied sites was tested. The refinement shows stability and a significant lowering of the reliabilities factors is obtained (drops from 4.84% to 3.95%). Whereas the result of such a "splitting" proves to be non-significant for the Ca-based compound, the situation is here quite different and one notices some improvements regarding the environment of the Ba atoms. For the sake of comparison, projections onto the ($y0z$) and ($x0y$) planes of the crystal structure obtained in the $F2mm$ space group is presented, respectively, in Figs. 2 and 3.

In a last stage of the refinement, based on the above mentioned SAED experiments and due to the large thermal displacement parameters obtained for some oxygen positions, a refinement using the space group $A2_1am$ was done. Only oxygen positions located in the middle of the perovskite blocks (namely O(1), O(2a), O(2b) and O(4) in Table 4) were allowed to evolve towards positions specific to this space group, all other positions were restricted to positions compatible with the $F2mm$ space group. Note that these results are in agreement with the NPD study in Ref. [8] where strong thermal displacement parameters are also observed for these same oxygen positions. This procedure allows actually to introduce a slight rotation of the TiO_6 octahedra located in the middle of the perovskite block (see, Fig. 3). No significant change was observed in the Ba/Bi repartition and the result is still different to the one proposed in [7 SG:$A21am$] and [8 SG:$F2mm$] but in agreement with the one proposed in [6 SG:$F2mm$]. The results proposed for the crystal structure of $BaBi_4Ti_4O_{15}$ are summarized in Table 4 and the main inter-atomic distances in the coordination sphere of the cationic sites in Table 5. Representations of the crystal structure projected onto the ($y0z$) and ($x0y$) planes are, respectively, in Figs. 2 and 3.

4. Discussion

In terms of layer stacking along the c-axis, both structures are closely related and exhibit the characteristics common to all Aurivillius phases. More precisely, A-site (Ca/Bi or Ba/Bi) and B-site (Ti) cations of the perovskite-like blocks are displaced along the c-axis in

Table 4
Refined structural parameters for $BaBi_4Ti_4O_{15}$ at 25°C $A2_1am$ (No. 36) with $a = 5.4433(4)$ Å, $b = 5.4319(6)$ Å, $c = 41.6941(3)$ Å. R indices [$I > 3\sigma(I)$/all data]: $R = 3.59\%/4.41\%$ and w$R = 3.24\%/3.25\%$

	Wickoff	x	y	z	U_{iso}	Occupancy
Bi(1)	8*b*	0.25[a]	0.25[b]	0.22076(2)	0.0126(2)[c]	0.895(5)
Ba(1)	8*b*	0.248(6)	0.25[b]	0.2066(3)	0.0126(2)[c]	0.105(5)
Bi(2)	4*a*	0.2845(7)	0.25[b]	0	0.0291(6)[c]	0.87(1)
Ba(2)	4*a*	0.188(4)	0.25[b]	0	0.0291(6)[c]	0.13(1)
Bi(3)	8*b*	0.2667(10)	0.25[b]	0.89258(3)	0.0262(4)[c]	0.67(1)
Ba(3)	8*b*	0.2191(14)	0.25[b]	0.89977(13)	0.0262(4)[c]	0.33(1)
Ti(1)	8*b*	0.2448(11)	0.25[b]	0.55000(5)	0.0053(6)	1
Ti(2)	8*b*	0.2434(14)	0.25[b]	0.34609(5)	0.0072(5)	1
O(1)	4*a*	0.711(3)	0.215(2)	0	0.018(5)	1
O(2*a*)[d]	8*b*	0.509(6)	0.469(3)	0.5483(4)	0.027(3)[c]	1
O(2*b*)[d]	8*b*	0.446(4)	-0.033(3)	0.5435(4)	0.027(3)[c]	1
O(3)	8*b*	0.999(4)	0.5[b]	0.25[b]	0.008(2)	1
O(4)	8*b*	0.223(3)	0.242(3)	0.4051(2)	0.021(3)	1
O(5*a*)[d]	8*b*	0.489(3)	0.5[b]	0.35625(12)	0.016(2)[c]	1
O(5*b*)[d]	8*b*	0.489(3)	0[b]	0.35625(12)	0.016(2)[c]	1
O(6)	8*b*	0.246(5)	0.25[b]	0.69515(18)	0.016(2)	1

Fractional coordinates and thermal parameters (Å^2).
[a] Fixed coordinate (polar space group).
[b] Fixed coordinate (derived from the *F2mm* space group).
[c] Thermal displacement parameter constraint to the same value.
[d] Oxygen positions originating from one single atomic position in the *F2mm* space group.

Table 5
Main interatomic distances in the coordination sphere (<3 Å) of Bi, Ba and Ti atomic positions

Ti(1)–O(1)	2.101(3) Å × 1	Ti(2)–O(4)	2.461(9) Å × 1
Ti(1)–O(2*a*)	1.87(3) Å × 1	Ti(2)–O(5*a*)	1.95(2) Å × 1
Ti(1)–O(2*a*)	2.00(3) Å × 1	Ti(2)–O(5*a*)	1.99(2) Å × 1
Ti(1)–O(2*b*)	1.89(2) Å × 1	Ti(2)–O(5*b*)	1.95(2) Å × 1
Ti(1)–O(2*b*)	2.03(2) Å × 1	Ti(2)–O(5*b*)	1.98(2) Å × 1
Ti(1)–O(4)	1.878(9) Å × 1	Ti(2)–O(6)	1.719(8) Å × 1
Bi(1)–O(3)	2.280(13) Å × 2	Ba(1)–O(3)	2.64(2) Å × 4
Bi(1)–O(3)	2.273(13) Å × 2	Ba(1)–O(6)	2.757(2) Å × 3
Bi(1)–O(6)	2.918(3) Å × 2	Ba(1)–O(6)	2.77(4) Å × 1
Bi(1)–O(6)	2.91(2) Å × 1	Ba(1)–O(6)	2.75(4) Å × 1
Bi(1)–O(6)	2.94(2) Å × 1		
Bi(2)–O(2*b*)	2.33(2) Å × 2	Ba(2)–O(2*b*)	2.58(2) Å × 2
Bi(2)–O(2*a*)	2.78(2) Å × 2	Ba(2)–O(2*b*)	2.72(2) Å × 2
Bi(2)–O(2*a*)	2.80(2) Å × 2	Ba(2)–O(2*a*)	2.54(2) Å × 2
Bi(2)–O(1)	2.330(15) Å × 1	Ba(2)–O(1)	2.61(3) Å × 1
Bi(2)–O(1)	2.555(13) Å × 1	Ba(2)–O(1)	2.85(3) Å × 1
Bi(2)–O(1)	2.935(13) Å × 1	Ba(2)–O(1)	2.526(13) Å × 1
		Ba(2)–O(1)	2.911(13) Å × 1
Bi(3)–O(4)	2.82(2) Å × 1	Ba(3)–O(4)	2.77(2) Å × 1
Bi(3)–O(4)	2.73(2) Å × 1	Ba(3)–O(4)	2.68(2) Å × 1
Bi(3)–O(4)	2.538(14) Å × 1	Ba(3)–O(4)	2.75(2) Å × 1
Bi(3)–O(5a)	2.37(1) Å × 1	Ba(3)–O(4)	2.71(2) Å × 1
Bi(3)–O(5*a*)	2.53(2) Å × 1	Ba(3)–O(5*a*)	2.701(11) Å × 1
Bi(3)–O(5*b*)	2.37(1) Å × 1	Ba(3)–O(5*a*)	2.59(1) Å × 1
Bi(3)–O(5*b*)	2.53(2) Å × 1	Ba(3)–O(5*b*)	2.701(11) Å × 1
		Ba(3)–O(5*b*)	2.59(1) Å × 1
		Ba(3)–O(2*a*)	2.72(2) Å × 1
		Ba(3)–O(2*b*)	2.92(2) Å × 1

the direction of the oxygen layers belonging to the $[M_2O_2]$ slabs (M = Bi or Bi/Ba). The displacement is less pronounced while going away from this $[M_2O_2]$ slabs. This expansion of the cationic sublattice is combined with a compression of the anionic sublattice along the z direction. As detailed in [4], if we consider these compounds as $AB_{1-x}O_3$ deficient perovskite, this appears as a natural consequence of the fact that while there exists less cationic layers both cationic and anionic sublattices have the same periodicity along the z direction. This tendency lead to the existence of some short Ti–O distances (notably Ti(2)–O(6)). In the cuboctaedral cavities, the displacement of A-site cations along the c-axis results in a move off the center of their respective polyhedrons towards one of its square faces as illustrated for $CaBi_4Ti_4O_{15}$ in Fig. 5. As shown in Fig. 3, the A-site cations are also moved along the polar axis a.

As evidenced from the refinement, one first difference between the two compounds is found in terms of structural distortions with respect to the prototype structure ($I4/mmm$): the $[A_{n-1}B_nO_{3n+1}]^{2-}$ perovskite blocks are more distorted in $CaBi_4Ti_4O_{15}$ than in $BaBi_4Ti_4O_{15}$, as seen in Figs. 2 and 3. This can be understood considering the average effective ionic radii of A cation. As indicated in [11] and then further developed in [3], it was shown on a broad range of Aurivillius phases that the structural distortion (and T_c) increases as the perovskite tolerance factor $t = (R_A + R_O)/\sqrt{2}(R_B + R_O)$ decreases. Considering the average ionic radii of the A-site cation $t = 0.957$ and 0.989 for $CaBi_4Ti_4O_{15}$ and $BaBi_4Ti_4O_{15}$, respectively

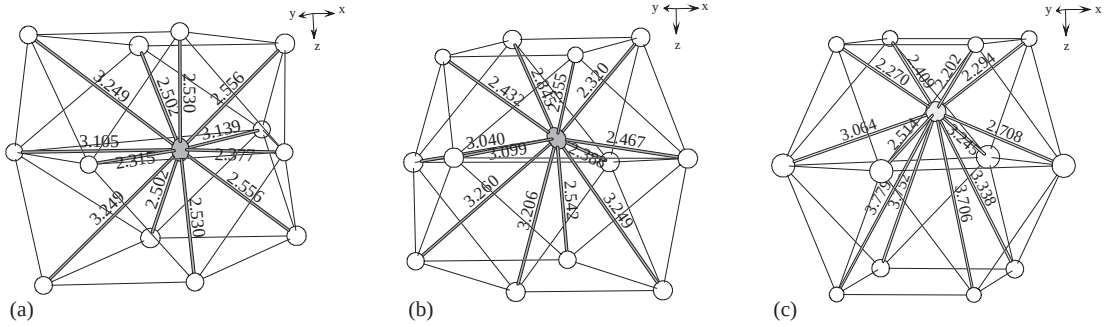

Fig. 5. Cuboctaedral cavities observed in $CaBi_4Ti_4O_{15}$: for the mixed Bi/Ca(2) and Bi/Ca(3) sites, respectively in (a) and (b). In (c) the location of Bi(1) in the cuboctaedral cavity is represented. The size of the spheres or ellipsoids used to represent the atomic positions correspond, respectively, to the isotropic or anisotropic thermal displacement parameters.

Table 6
Average distances and bond valence sums (BVS), experimental and theoretical, for the *A*-sites of $ABi_4Ti_4O_{15}$ (this study) and $ABi_2Nb_2O_9$ [14] (A = Ca, Ba)

	$BaBi_4Ti_4O_{15}$					$CaBi_4Ti_4O_{15}$			
	$\langle A\text{–O}\rangle_{exp.}$ (Å)	$\langle A\text{–O}\rangle_{th.}$ (Å)	$V_{exp.}$	$V_{th.}$		$\langle A\text{–O}\rangle_{exp.}$ (Å)	$\langle A\text{–O}\rangle_{th.}$ (Å)	$V_{exp.}$	$V_{th.}$
Bi(1) [4+4]	2.60	2.57	2.92	3	Bi (1) [4+2]	2.40	2.43	3.07	3
Ba(1) [8]	2.70	2.82	2.94	2					
Bi(2) [4+5]	2.63	2.64[a]	2.80	3	Bi(2) [8]	2.48	2.57	3.10	3
Ba(2) [10]	2.66	2.92	4.10	2	Ca(2) [8]	2.48	2.52	2.20	2
Bi(3) [5+2]	2.55	2.50[a]	2.49	3	Bi(3) [6+1]	2.48	2.50[a]	2.96	3
Ba(3) [10]	2.71	2.92	3.47	2	Ca(3) [6+1]	2.48	2.46	2.10	2
	$BaBi_2Nb_2O_9$					$CaBi_2Nb_2O_9$			
	$\langle A\text{–O}\rangle_{exp.}$ (Å)	$\langle A\text{–O}\rangle_{th.}$ (Å)	$V_{exp.}$	$V_{th.}$		$\langle A\text{–O}\rangle_{exp.}$ (Å)	$\langle A\text{–O}\rangle_{th.}$ (Å)	$V_{exp.}$	$V_{th.}$
Bi/Ba(2) [4+4]	2.65	2.60	2.84	2.87	Bi/Ca(2) [4+2]	2.40	2.43	2.96	2.95
Bi/Ba(1) [12]	2.80	2.92	2.65	2.26	Bi/Ca(1) [10]	2.48	2.523	2.32	2.10

The theoretical bond distances were calculated using the effective ionic radii (Ref. [12]) corresponding to the observed coordination number at 3 Å (Table 5) and indicated in square brackets for each *A*-site. BVS were calculated by taking into consideration all the *A*–O distances up to the coordination number [12].

[a] Ionic radius of Bi^{3+} with a co-ordination number [7] estimated by interpolation (Ref. [12]).

($R_{O^{2-}} = 1.40$ Å, $R_{Ti^{4+}(VI)} = 0.605$ Å, $R_{Ba^{2+}(XII)} = 1.61$ Å, and $R_{Ca^{2+}(XII)} = 1.34$ Å from [12] and $R_{Bi^{3+}(XII)} = 1.30$ Å as estimated in [3]).

For $CaBi_4Ti_4O_{15}$, the octahedra are rotated along the *a*- and *c*-axis, alternatively in opposite directions. No rotations along the *b*-axis are observed. Such tilting of the octahedra results from the just mentioned capacity of the perovskite blocks to accommodate, within the cuboctaedral cavities, *A*–O distances compatible with a *A*-site cation less voluminous than the ideal one ($t<1$). The reduction of some distances in the cuboctaedral cavities allows to get acceptable anionic environments for both Ca^{2+} and Bi^{3+} cations. It follows (see, Table 3) that the actual coordination number drops to [8] and [6+1], respectively, for the Bi/Ca(2) and Bi/Ca(3) sites instead of [12] in the ideal prototype structure. Considering this (see, Table 6), the average $\langle A\text{–O}\rangle$ distances and bond valences for the Bi/Ca(2) and Bi/Ca(3) sites are in good agreement with the ones expected for such a coordination number. Also, the bond valences measured for Bi and Ca show that these sites are acceptable for both Bi^{3+} and Ca^{2+} cations. On the contrary, the Bi(1) site ($[Bi_2O_2]$ slab) with its [4+2] coordination number and four short Bi–O distances (2.2–2.4 Å) is clearly not compatible with Ca^{2+} cations.

For $BaBi_4Ti_4O_{15}$, the oxygen environment of the *A*-sites located within the perovskite blocks poses problems for Ba^{2+}. From the refinement and on a crystal chemistry point of view, the separation of Bi and Ba cations in two different sites of the same cuboctahedral cavity appears as a necessity. This result shows similarities with the oxygen deficient perovskites $(Ba_{2-3x}Bi_{3x-1})(Fe_{2x}Bi_{1-2x})O_{2+3/2x}$ [13], where a true Ba/Bi statistical occupancy of one single *A* site was proved to be impossible and distinct atomic positions have to be considered. Considering such a "splitting", the Ba^{2+} cations, more voluminous than Bi^{3+}, present

then more regular anionic environments and higher coordination numbers (Table 5). This constitutes undoubtedly an improvement compared to a model where anisotropic thermal displacement parameters would be refined for mixed Ba/Bi sites. Nonetheless the coordination number and the bond valences obtained (Table 6) are still not as satisfactory as for the Ca-based compound, which shows the limit of such an "average" crystal structure determination. Hence, the observed average $\langle$ Ba–O $\rangle$ distances are still much shorter than the expected ones. Ba cations are thus clearly and systematically overbonded, especially for the Ba(2) site. Such a situation was already observed for $BaBi_2Nb_2O_9$ ($n = 2$) [14].

Another major difference between the two compounds is the presence of a significant amount of Ba cations into the $[M_2O_2]$ specific slabs for $BaBi_4Ti_4O_{15}$. It results that even though the Bi/A' ratio remains very similar for the Bi/A'(3) sites, the A' content of the Bi/A'(2) sites in $CaBi_4Ti_4O_{15}$ is almost equally redistributed in both Ba(2) and Ba(1) sites in $BaBi_4Ti_4O_{15}$ (Tables 2 and 4). Considering the separation of Bi and Ba sites, the Ba(1) sites located in the cuboctahedral cavities generally occupied by Bi in the $[M_2O_2]$ slabs are actually less overbonded than Ba(2) (Table 6). It must be noticed that the presence of Ba cations in the $[M_2O_2]$ slabs is also observed in $BaBi_2Nb_2O_9$ ($n = 2$) [14–16] even if Bi and Ba positions have not been distinguished in the refinement of this structure. On the contrary for $Bi_{1.8}Sr_{2.2}Ti_{0.8}Nb_{2.2}O_{12}$ ($n = 3$) [17], where Sr cations are present in the $[M_2O_2]$ slabs, two distinct Bi- and Sr-sites are evidenced.

Regarding the ferroelectric properties of these compounds, they exhibit Curie temperatures of 790°C for $CaBi_4Ti_4O_{15}$ with a sharp transition ("normal" ferroelectric behavior) [18] and 390°C for $BaBi_4Ti_4O_{15}$ with a broad transition (relaxor-like ferroelectric behavior) [18]. When the difference in T_c can be related to the different level of structural distortion with respect to the prototype structure, the difference observed in the ferroelectric behavior is more difficult to explain. The present structural comparative analysis of $CaBi_4Ti_4O_{15}$ and $BaBi_4Ti_4O_{15}$ shows that, for this last compound, the Bi^{3+} and Ba^{2+} cations have specific anionic environments and cannot share identical atomic positions. The strong overbonding observed for the Ba^{2+} cations reflects structural stresses in the structure. A certain stress relief can be assure considering local configurations with compositional fluctuations and where octahedral tiltings will be less pronounced for Ba-rich zones (locally $t_{max.}$ up to 1.06) than for Bi-rich zones ($t_{min.} = 0.95$). Such a possibility is strongly supported by the observation of diffuse streaks in the SAED patterns (Fig. 4), related to the $A2_1am$ space group. This space group is, indeed, a signature of the double tilt system (along the a- and c-axis) usually observed in the even layer Aurivillius compounds contrary to $F2mm$, which did not allow any octahedra tiltings. Observation in NPD patterns [7] of reflections specific to the $A2_1am$ space group did actually not allow to assert that all the powder was homogeneous and is thus not a contradictory argument.

Following this, the particularities of the Ba-based compound can be considered in view of the conventional description of relaxor behavior in ferroelectrics [19]:

- the drastically different bounding requirement of Ba and Bi cations implies the existence of distinct atomic positions for each of them which is not the case for related Ca- and Sr-based compounds. The compositional fluctuations are here clearly associated to positional fluctuations of the A-site cations from one cell to the other. Also, considering the large difference in the ionic radii of Ba^{2+} and Bi^{3+} cations, locally the tolerance factor would be strongly affected by such local changes in the Ba/Bi ratio. For zones with high content in Ba, this may lead locally to undistorted structure and eventually non-polar domains. The combination of these two arguments, related to the composition fluctuation, is certainly of importance to explain the particular ferroelectric behavior of this Ba-based Aurivillius phase.
- the diffraction data analyses evidence a certain degree of disorder which is both in the form of composition and position fluctuations (static disorder and stacking faults). The fact that the phase transition observed for this compound occurs at low temperature (<400°C) is likely to freeze these disorders and generate a diffuse transition. Again this is a major difference with other $A'Bi_4Ti_4O_{15}$ related Aurivillius compounds.

5. Conclusion

The comparative single crystal X-ray diffraction study of these $n = 4$ Ba- and Ca-based Aurivillius phases allowed us to evidence the differences between these two compounds. In this respect $CaBi_4Ti_4O_{15}$ should be regarded as a representative example of a "classic" Aurivillius ferroelectric phase while $BaBi_4Ti_4O_{15}$ exhibits a relaxor behavior.

$CaBi_4Ti_4O_{15}$ and $BaBi_4Ti_4O_{15}$ have radically different cation environments, due to the difference in the ionic radii of the Ca^{2+} and Ba^{2+} cations. Regarding the $CaBi_4Ti_4O_{15}$ phase, in agreement with the tolerance factor, a significant deformation of the perovskite blocks is observed. The rotation system of the octahedra is typical of that observed in the Aurivillius phases and lead to the use of the space group $A2_1am$. Mixed Bi/Ca atomic positions exist within the perovskite blocks but specific Ca or Bi sites cannot be evidenced.

Regarding the $BaBi_4Ti_4O_{15}$ phase, most of the previous crystallographic studies [5–7] have demonstrated the necessity to partially substitute Bi for Ba in the $[M_2O_2]$ slabs to account for the experimental diffraction data. Even if this appears to be a particularity of this Ba-based compound, the relation with the relaxor behavior was still not obvious. Actually most of the Aurivillius phase possess atomic positions with a mixed occupancy (on the *A* and/or *B* site of the perovskite blocks) without being associated with a relaxor behavior. The present work shows that, in addition, one has to consider the existence of distinct atomic positions for the Ba and Bi cations. Such positional static disorder associated with the composition fluctuations should be responsible to the ferroelectric relaxor behavior through the formation of microdomains with different structural distortion levels. Similar arguments are developed in [11] to explain the relaxor-type ferroelectric transition observed in $BaBi_2Ta_2O_9$.

Lastly, questions have still to be answered regarding the local structural effects associated to the presented "average" crystal structure of $BaBi_4Ti_4O_{15}$. Notably, we believe that the presence of a significant amount of foreign cations into the $[Bi_2O_2]$ specific slabs such as Ba^{2+} for $BaBi_4Ti_4O_{15}$ should be regarded as representative of an averaging effect of the macroscopic crystal structure analysis. The incompatibility between the Ba^{2+} anionic environment and the configuration of the $[Bi_2O_2]$ slabs is so important that, at a local scale, the continuity of the $[Bi_2O_2]$ slabs cannot be ensure. Existence of faults or mismatch in the layers stacking within the crystal have to be present as illustrated for instance by the staircase type defects observed in thin films of the $n = 5$ $Ba_2Bi_4Ti_5O_{18}$ Aurivillius phase [20].

References

[1] B. Aurivillius, Arkiv. Kemi 1 (1949) 463, 499.
[2] R.L. Withers, J.G. Thompson, A.D. Rae, J. Solid State Chem. 94 (1991) 404.
[3] D.Y. Suarez, I.M. Reaney, W.E. Lee, J. Mater. Res. 11 (2001) 3139.
[4] Ph. Boullay, G. Trolliard, D. Mercurio, L. Elcoro, J.M. Perez-Mato, J. Solid State Chem. 164 (2002) 261.
[5] G. Nalini, T.N. Guru Row, Bull. Mater. Sci. 4 (2002) 275.
[6] M.E. Fuentes, A. Mehta, L. Lascano, H. Camacho, R. Chianelli, J.F. Fernandez, L. Fuentes, Ferroelectrics 269 (2002) 159.
[7] B.J. Kennedy, Y. Kubota, B.A. Hunter, K. Ismundar, Kato, Solid State Commun. 126 (2003) 653.
[8] Ph. Lightfoot, A. Snedden, S.M. Blake, K.S. Knight, Mater. Res. Soc. Symp. Proc. 755 (2003) 89.
[9] V. Petricek, M. Dusek, The Crystallographic Computing System JANA2000, Institute of Physics, Academy of Sciences of the Czech Republic, Praha, 2000.
[10] C.H. Hervoches, A. Snedden, R. Riggs, S.H. Kilcoyne, P. Manuel, Ph. Lightfoot, J. Solid State Chem. 164 (2002) 280.
[11] Y. Shimakawa, Y. Kubo, Y. Nakagawa, S. Goto, T. Kamiyama, H. Asano, F. Izumi, Phys. Rev. B 61 (2000) 6559.
[12] R.D. Shannon, C.T. Prewitt, Acta. Crystallogr. A 32 (1976) 751.
[13] Ph. Boullay, D. Grebille, M. Hervieu, B. Raveau, J. Solid State Chem. 147 (1999) 450.
[14] S.M. Blake, M.J. Falconer, M. McCreedy, Ph. Lightfoot, J. Mater. Chem. 7 (1997) 1609.
[15] B.J. Ismunandar, Kennedy, J. Mater. Chem. 9 (1999) 541.
[16] R. Macquart, B.J. Kennedy, Y. Shimakawa, J. Solid State Chem. 160 (2001) 174.
[17] C.H. Hervoches, Ph. Lighfoot, J. Solid State Chem. 153 (2000) 66.
[18] G.A. Smolenski, V.A. Bokov, V.A. Isupov, N.N. Krainik, R.E. Pasynkov, A.I. Sokolov, Ferroelectrics and Related Materials, in: G.A. Smolenski (Ed.), Gordon and Breach Science Publishers, London, 1984.
[19] M.E. Lines, A.M. Glass, Principles and Applications of Ferroelectrics and Related Materials, Oxford University Press, Oxford, 1977.
[20] D. Hesse, N.D. Zakharov, A. Pignolet, A.R. James, S. Senz, Cryst. Res. Technol. 35 (2000) 641.